

A FAST TOUR DESIGN METHOD USING NON-TANGENT V-INFINITY LEVERAGING TRANSFERS

Stefano Campagnola * Nathan J. Strange † and Ryan P. Russell ‡

The announced missions to the Saturn and Jupiter systems renewed the space community interest in simple design methods for gravity assist tours at planetary moons. A key element in such trajectories are the V-Infinity Leveraging Transfers (VILT) which link simple impulsive maneuvers with two consecutive gravity assists at the same moon. VILTs typically include a tangent impulsive maneuver close to an apse location, yielding to a desired change in the excess velocity relative to the moon. In this paper we study the VILT solution space and derive a linear approximation which greatly simplifies the computation of the transfers, and is amenable to broad global searches. Using this approximation, Tisserand graphs, and heuristic optimization procedure we introduce a fast design method for multiple-VILT tours. We use this method to design a trajectory from a highly eccentric orbit around Saturn to a 200 km science orbit at Enceladus. The trajectory is then recomputed removing the linear approximation, showing a Δv change of less than 4%. The trajectory is 2.7 years long and comprises 52 gravity assists at Titan, Rhea, Dione, Tethys, and Enceladus, and several deterministic maneuvers. Total Δv is only 445 m/s, including the Enceladus orbit insertion, almost 10 times better than the 3.9 km/s of the Enceladus orbit insertion from the Titan-Enceladus Hohmann transfer. The new method and demonstrated results enable a new class of missions that tour and ultimately orbit small mass moons. Such missions were previously considered infeasible due to flight time and Δv constraints.

INTRODUCTION

The method of V-Infinity Leveraging Transfers (VILTs) has received new attention because of recently announced plans to send spacecraft to orbit planetary moons in the Jupiter and Saturn systems. The trajectory design of such missions typically includes a complex sequence of maneuvers and gravity assists at the moons to efficiently solve the endgame problem of reducing the orbit insertion Δv .

VILTs are used to modify the gravity assist v_∞ with maneuvers. These transfers are built around the concept of a *leveraging maneuver** which generalizes the concept of a $\Delta V - EGA$ (i.e. using a ΔV between Earth flybys to increase the effective launch energy). Leveraging maneuvers work by increasing the eccentricity of the orbit around the central body to increase flyby v_∞ . Conversely, the flyby v_∞ is decreased when the leveraging maneuver reduces orbit eccentricity.

VILTs have been implemented in several missions³⁻⁶ and are the subject of several papers.⁷⁻¹³ The VILT is primarily used to efficiently increase or decrease excess hyperbolic velocity relative to a planet or planetary moon. Recent work¹⁰ has shown that leveraging can also be used to effectively increase the bending available from flybys of low mass moons. This new application can be used to construct gravity-assist tours with low mass moons that avoid degenerate, long flight-time, resonances (e.g. it can enable reaching a 1:1 resonance when, at best, only a 19:18 resonance could be reached ballistically).

*Ph.D. candidate, University of Southern California, Aerospace and Mechanical Engineering, 854 Downay Way RRB, Los Angeles, CA 90089-1191, stefano.campagnola@missionanalysis.org

†Senior Engineer, Jet Propulsion Laboratory / California Institute of Technology, 4800 Oak Grove Drive, Pasadena, CA 91109

‡Assistant Professor, Georgia Institute of Technology, Guggenheim School of Aerospace Engineering, 270 Ferst Drive, Atlanta, GA 30332-0150, ryan.russell@gatech.edu

*V-infinity “leveraging” is a term first coined by Longuski and first documented by Williams.¹ It is intended to evoke the gravity-assist tour design terminology of “pumping” (changing orbit period) and “cranking” (changing orbit inclination).²

In this paper, we derive a fast linear approximation that avoids the iterative solution for VILTs required previously.¹⁰ This fast approximation facilitates the investigation of a broader set of possible tours constructed from VILTs, and consequently, the discovery of better trajectories. One first example of this was the solution presented in a previous paper.¹⁰ Here we present the graphical method used for the design of that solution and also present a second solution, with a substantial improvement of the total Δv .

The first section of this paper studies the general VILT problem and its solution space. The main steps of the section are (1) demonstrate that the solution space is almost flat for a specific choice of coordinates, (2) construct approximated solutions using minimal memory storage. In the second section we exploit the large reduction in complexity and computational time resulting from this approximation to develop a new design method amenable for broad design space searches. In the third section we present the Enceladus orbiter trajectory.

VILT

V-infinity leveraging transfers (VILTs) are trajectories around a major body (e.g., a planet) that start and end at a minor body (e.g., a moon) and include one small impulsive maneuver (Δv) to achieve a large change in the spacecraft velocity relative to the minor body (v_∞). VILTs are usually modeled with two Keplerian arcs patched by a tangential Δv at the leveraging apse r_{LA}^* , while the moon is in a circular coplanar orbit. In most of the literature, one of the two Keplerian transfers is assumed tangent to the moon's orbit (*tangent VILT*) to both simplify the analysis and to achieve a near optimal increase or decrease in v_∞ at the moon.¹⁴

In cases where VILTs are patched together with flybys of non-massive bodies, the tangent VILT is very inefficient in terms of flight time due to geometry of the flyby. As demonstrated in Figure 1, the impulsive Δv vector associated with a gravity assist beginning with the tangent geometry is almost perpendicular to the spacecraft velocity, thereby leaving the magnitude of the velocity relative to the central body almost unchanged. Whereas in the case of the non-tangent flyby geometry, the Δv vector goes almost entirely towards changing the velocity magnitude. In the limit as the available turn angle approaches zero, the tangent geometry flyby provides no change in energy while the most efficient energy change occurs in the non-tangent case with pump angle equal to $(\pi - \arccos v_\infty)$. Following the work of Strange et al.,¹⁰ this lack of efficiency for VILTs constrained by small turn angles motivates us to remove the tangent assumption.

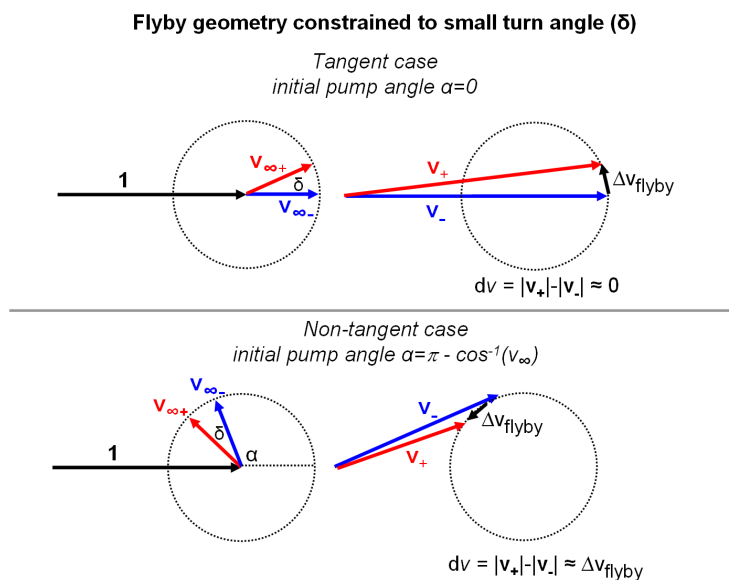


Figure 1. Geometry of the gravity assists when the turn angle is small

*The symbols are explained in the Notation section at the end of the paper.

We normalize the distances and the times with the scale factors $l^* = \tilde{a}_M$ and $t^* = \sqrt{\tilde{a}_M^3 / \tilde{\mu}_P}$, where the tilde denotes the dimensioned variables. As a result of the normalization, $\mu_P = 1$, $v_M = 1$ and the VILTs start and end at $r = 1$. We model the gravity assist as usual by linking two consecutive VILTs with an instantaneous rotation of the v_∞ vector by the turning angle $\delta = 2 \arcsin(\tilde{\mu}_M / (\tilde{\mu}_M + \tilde{v}_\infty^2 \tilde{r}_\pi))$, where \tilde{r}_π is the pericenter of the gravity assist. This is sometimes called zero sphere-of-influence gravity assist.

Classification and special solutions

We classify the VILTs with the parameter vector $s = (\sigma_1, k_1, \sigma_2, k_2, EI, n)$ and the notation:

$$(EI) n : m_{k_1, k_2}^{\sigma_1, \sigma_2}$$

where $m = k_1 + k_2 + 1$ is the number of spacecraft revolutions and the elements of p are:

$$k_i \quad i = 1, 2 \quad \text{Number of full revolutions in the } i\text{th arc}$$

$$\sigma_i = \begin{cases} -1 & \text{Short transfer } 2k_i\pi < \Delta\theta < \pi + 2\pi k_i \\ +1 & \text{Long transfer } \pi + 2\pi k_i < \Delta\theta < 2\pi + 2\pi k_i \end{cases}$$

$$EI = \begin{cases} -1 & \text{Interior VILT } (\Delta v \text{ at apoapsis}) \\ +1 & \text{Exterior VILT } (\Delta v \text{ at periapsis}) \end{cases}$$

$$n \quad \text{Number of moon revolutions}$$

Figure 2 shows an example of an exterior VILT on the left, and explains the notation for the first arc on the right. In the figure the leveraging apse r_{LA} is the apocenter, while the vacant apse r_{VA} (opposite to the leveraging apse) is the pericenter.

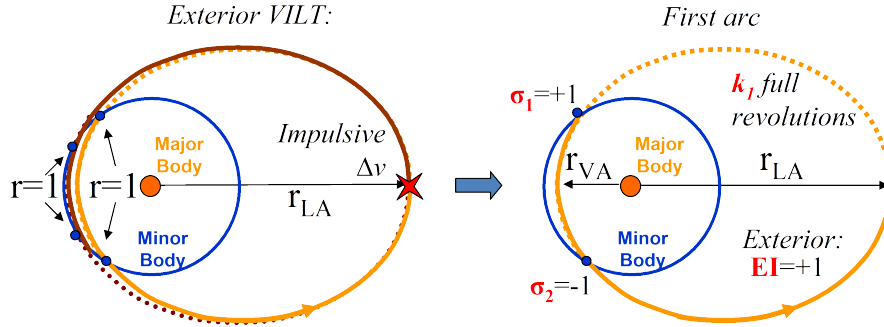


Figure 2. Example of exterior VILT on the left. On the right, the first arc of the VILT

A special family of VILTs is the family of tangent VILTs, described in Campagnola and Russell¹² with the notation $n : m^{\bar{\sigma}}(\bar{k})$, where $\bar{\sigma}, \bar{k}$ refers to the non-tangent arc. Note that $n : m^{\bar{\sigma}}(\bar{k})$ is a special case of a $(EI) n : m_{k_1, k_2}^{\sigma_1, \bar{\sigma}}$ VILT (first arc tangent to the moon's orbit) and of a $(EI) n : m_{k, k_2}^{\bar{\sigma}, \sigma_2}$ VILT (second arc tangent to the moon's orbit).

A second special family of VILT is the family of ballistic transfers, where $\Delta v = 0$ implies $r_{VA1} = r_{VA2}$. We classify the ballistic transfers with the notation $n : m^{\bar{\sigma}}$, where $\bar{\sigma} = 0$ corresponds to the ballistic *resonant* transfers, and $\bar{\sigma} = \pm 1$ correspond to nonresonant transfers with slightly more or fewer than m revolutions, respectively (also called generic or non- $n\pi$ returns). Note that $n : m^{\pm 1}$ is a special case of a $(EI) n : m_{k_1, k_2}^{\pm 1, \pm 1}$ VILT, while $n : m^0$ is a special case of a $(EI) n : m_{k_1, k_2}^{\pm 1, \mp 1}$ VILT.

Phasing constraint

Using our notation, the true and mean anomaly spanned by the spacecraft in either arc are (see also Strange at al.¹⁰):

$$\Delta f^{(\sigma_i, k_i, EI)} = 2\pi k_i - f|_{r=1}^{(\sigma_i, EI)} + \pi[1 + \sigma_i(EI - 1)/2] \quad i = 1, 2 \quad (1)$$

$$\Delta M^{(\sigma_i, k_i, EI)} = 2\pi k_i - M|_{r=1}^{(\sigma_i, EI)} + \pi[1 + \sigma_i(EI - 1)/2] \quad i = 1, 2 \quad (2)$$

where $f|_{r=1}^{(\sigma_i, EI)} \in (-\pi, \pi]$ and $M|_{r=1}^{(\sigma_i, EI)} \in (-\pi, \pi]$ are the true and mean anomaly of the spacecraft at the moon. Using Eq.(1) and Eq.(2) we define the *spacecraft angular gain* :

$$(\Delta\theta)_i = \Delta f^{(\sigma_i, k_i, EI)} - a_i^{3/2} \Delta M^{(\sigma_i, k_i, EI)} \quad i = 1, 2 \quad (3)$$

where the second term is the true anomaly spanned by the moon , which is also the transfer time.

Due to the symmetry of the problem, each of the two arcs composing the VILT is completely defined with only two independent variables (*coordinates*), like (a_i, e_i) or (r_{ai}, r_{pi}) or $(v_{\infty i}, r_{LAi})$, $i = 1, 2$. Thus four coordinates completely define the VILT. However, as we patch the two arcs together, the VILT coordinates must satisfy the *apsis constraint equation*:

$$r_{LA1} = r_{LA2} \quad (4)$$

Also, the true anomaly spanned by the moon must equal the true anomaly spanned by the spacecraft, modulo 2π . That is , the VILT must satisfy the *phasing constraint equation*¹⁰ :

$$(\Delta\theta)_1 + (\Delta\theta)_2 = 2\pi(k_1 + k_2 + 1 - n) \quad (5)$$

For a choice of the VILT parameter vector $s = (\sigma_1, k_1, \sigma_2, k_2, EI, n)$ and under certain regularity conditions which we do not discuss here, the Submersion Theorem¹⁵ applied to Eq.(4) and Eq.(5) shows that the solution space of the VILT is a two-dimensional differentiable manifold. In other words, we have a four dimensional space with two constraints leaving two degrees of freedom. We denote the *VILT manifolds* with the notation \mathcal{V}^s , where s is the VILT parameter vector.

Coordinates

In this section we introduce some choice of coordinates (independent variables) which describes a Keplerian arc. In the next section we use these coordinates to write the constraint equations (4-5), i.e. to define the embedding space and compute the VILT manifold.

If we choose (r_a, r_p) as coordinates, many orbital parameters take a very simple form, as shown in Table 1. The formulas* in Table 1 are derived using the conservation of momentum and energy.

Another two choices of coordinates are (r_{LA}, v_{∞}) and (r_{LA}, r_{VA}) , for which we derive the following coordinate transformations:

$$\varphi : (r_{LA}, r_{VA}) \mapsto (r_a, r_p) = \begin{cases} (r_{LA}, r_{VA}) & \text{if } EI = +1 \\ (r_{VA}, r_{LA}) & \text{if } EI = -1 \end{cases} \quad (6)$$

and

*In the table, the third third row comes from $v_{\infty}^2 = 1 + v|_{r=1}^2 - 2h = 1 + (2 - \frac{1}{a}) - 2\sqrt{p}$. The fourth row uses the trigonometry identity $\tan \frac{f}{2} = \pm \sqrt{\frac{1 - \cos f}{1 + \cos f}}$. The fifth row uses the trigonometry identity $\sin E = 2 \frac{\tan(E/2)}{1 + \tan^2(E/2)}$.

Table 1. Some useful two-body mechanics formulas as functions of r_a, r_p in normalized variables

(a, e, p)	$\left(\frac{r_a+r_p}{2}, \frac{r_a-r_p}{r_a+r_p}, \frac{2r_a r_p}{r_a+r_p} \right)$
(v_a, v_p)	$\left(\sqrt{\frac{r_p}{r_a} \frac{2}{(r_a+r_p)}}, \sqrt{\frac{r_a}{r_p} \frac{2}{(r_a+r_p)}} \right)$
v_∞	$\sqrt{3 - \frac{2}{r_a+r_p} - 2\sqrt{\frac{2r_a r_p}{r_a+r_p}}}$
$f _{r=1}^{(\sigma_i, EI)}$	$(-\sigma EI) \arccos\left(\frac{2r_a r_p - r_a - r_p}{r_a - r_p}\right)$ and $(-\sigma EI) 2 \arctan\left(\sqrt{\frac{r_a}{r_p} \frac{(1-r_p)}{(r_a-1)}}\right)$
$E _{r=1}^{(\sigma_i, EI)}$	$(-\sigma EI) \arcsin\left(2\sqrt{\frac{(1-r_p)(r_a-1)}{r_a-r_p}}\right)$ and $(-\sigma EI) 2 \arctan\left(\sqrt{\frac{(1-r_p)}{(r_a-1)}}\right)$
$M _{r=1}^{(\sigma_i, EI)}$	$(-\sigma EI) \left[2 \arctan\left(\sqrt{\frac{(1-r_p)}{(r_a-1)}}\right) - 2\sqrt{\frac{(1-r_p)(r_a-1)}{r_a+r_p}} \right]$

$$\psi : (r_{LA}, v_\infty) \mapsto (r_{LA}, r_{VA}) \quad (7)$$

where r_{VA} is given by Eqs.(8) and (9)*

$$v_{LA} = r_{LA} - EI \sqrt{r_{LA}^2 - 3 + \frac{2}{r_{LA}} + v_\infty^2} \quad (8)$$

$$r_{VA} = (2/(r_{LA} v_{LA})^2 - 1/r_{LA})^{-1} \quad (9)$$

(r_a, r_p) Tisserand Graph

The $r_a - r_p$ Tisserand graph [†], shown in Figure 3, is the domain (r_a, r_p) , $r_a > 1; r_p < 1$, where each point represents one Keplerian orbit in the orbital plane of the moon. In this domain we plot the v_∞ level sets, i.e. the family of curves $r_a(r_p; v_\infty)$ or $r_p(r_a; v_\infty)$ which we compute using Eqs.(8) and (9) and treating v_∞ as a parameter. Zero sphere-of-influence gravity assists and impulsive maneuvers are jumps on the graph. In particular, Figure 3 shows the effect of a tangent Δv at apocenter (pericenter respectively) that brings the spacecraft from the point B to the point C (D respectively). Figure 3 also shows a gravity assist that moves the spacecraft from the point A to the point B on the same v_∞ level set. Note that the gravity assist shift is limited by the minimum altitude constraint.

It was shown¹³ that the $r_a - r_p$ Tisserand graph is in fact the Tisserand-Poincaré (T-P) graph restricted to the $r_a > 1; r_p < 1$ domain. The T-P graph is a Poincaré section in the spacecraft-moon-planet three body problem with constant energy level sets (which are the v_∞ level sets in the Tisserand graph).

Solution space representation

In this section we use the coordinates introduced previously to represent the VILT solution space. Other choices of coordinates are possible.¹⁰

First we write the spacecraft angular gain of Eq.(3) as function of (r_a, r_p) using Table 1:

*From the conservation of energy and momentum we find the quadratic: $v_{LA}^2 - 2v_{LA}r_{LA} + 2\left(1 - \frac{1}{r_{LA}}\right) + 1 - v_\infty^2 = 0$. Using energy-based arguments we can pick the correct root, as shown in the formula. The second equation is derived from the conservation of energy.

[†]The Tisserand graph was originally introduced in a $(Period, r_p)$ plane.^{9,16} The (r_a, r_p) representation is much more useful for the leveraging transfer problem as the leveraging maneuvers move along lines of either constant r_p or constant r_a .^{10,12,13}

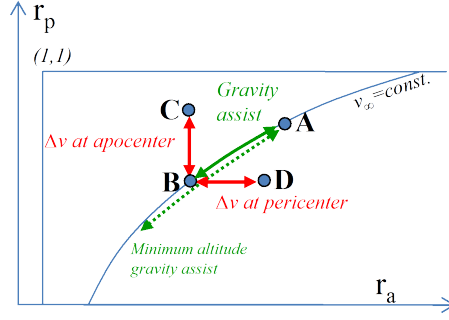


Figure 3. $r_a - r_p$ Tisserand graph (schematic) with the effects of a gravity assist and of tangent Δv s at pericenter or apocenter

$$\begin{aligned} \Delta\theta_{(\sigma,k,EI)}(r_a, r_p) = & 2\pi k + \sigma EI \arccos\left(\frac{2r_a r_p - r_a - r_p}{r_a - r_p}\right) + \pi[1 + \sigma(EI - 1)/2] + \\ & - \sqrt{\frac{(r_a + r_p)^3}{8}} \left(2\pi k + \sigma EI \left[2 \arctan\left(\sqrt{\frac{(1-r_p)}{(r_a-1)}}\right) - 2 \sqrt{\frac{(1-r_p)(r_a-1)}{r_a+r_p}} \right] + \pi[1 + \sigma(EI - 1)/2] \right) \end{aligned} \quad (10)$$

Then we choose the coordinates $(r_{LA}, v_{\infty 1})$ for the first arc and (r_{LA}, r_{VA2}) for the second arc, and write the phasing constraint Eq. (5) using Eq.(10) with the coordinate transformations Eq.(6-7):

$$\Delta\theta_{(\sigma_1, k_1, EI)} \circ \psi(r_{LA}, v_{\infty 1}) + \Delta\theta_{(\sigma_2, k_2, EI)} \circ \psi \circ \varphi(r_{LA}, r_{VA2}) - 2\pi(k_1 + k_2 + 1 - n) = 0 \quad (11)$$

where the circle \circ denotes function composition.

For a given VILT parameter vector s , we solve numerically Eq.(11) to compute the two dimensional manifold \mathcal{V}^s embedded in $(r_{LA}, r_{VA2}, v_{\infty 1})$. We also take sections of the manifold at $v_{\infty 1} = const$, which we denote as $\gamma_{v_{\infty 1}}^s$. From the Implicit Function Theorem,¹⁵ we know that the sections $\gamma_{v_{\infty 1}}^s$ can be written as curves

$$r_{LA}^s(r_{VA2}; v_{\infty 1}) \quad (12)$$

satisfying Eq.(11), which we can plot on a Tisserand graph.

The special families of VILTs described previously (ballistic and tangent VILTs) must satisfy one additional constraint equation ($r_{VA1} = r_{VA2}$ for the ballistic solution, $r_{VA1} = 1$ or $r_{VA2} = 1$ for tangent VILT) and are therefore one-dimensional subsets of \mathcal{V}^s .¹² Their intersections with $v_{\infty 1} = const$. are points.

Figure 4 shows the manifold $\mathcal{V}^{(1,0,-1,3,+1,5)}$ associated to the $(+1) 5 : 4_{0,3}^{1,-1}$ VILT, embedded in the $(r_a, r_{p2}, v_{\infty 1})$ space. It also shows the family of ballistic transfers $5 : 4^0$ and the VILTs tangent at departure $(+1) 5 : 4^{-1}(3)$ and at arrival $(+1) 5 : 4^{+1}(0)$. As expected, the tangent VILTs are the boundaries of the manifold. Note that the VILTs tangent at departure are not defined for $v_{\infty 1}$ greater than ~ 0.15 .

Figure 5 on the left shows a close up of the same manifold $\mathcal{V}^{(1,0,-1,3,+1,5)}$ and of the ballistic and tangent families. In the same space we plot the pericenters of the first arc r_{p1} as function of $(r_a, v_{\infty 1})$, which we compute using Eq.(8-9). The plane $v_{\infty 1} = 0.12$ generates the section $\gamma_{v_{\infty 1}}^s$, or equivalently the curve $r_{p2} = (r_a; v_{\infty 1})$, and the curve $r_{p1}(r_a; v_{\infty 1})$, i.e. the $v_{\infty 1}$ level set of the Tisserand graph. The plane also intersects the ballistic and tangent VILTs in the points $P1, P2, P3$. The point $P2$ represents the ballistic transfer, i.e. the solution with $r_{p1} = r_{p2}$. Figure 5 on the right shows the same section as a Tisserand graph. It is effectively a rotated frontal view of the 3D plot. In this example, the tangent VILTs are the vertical jumps from the r_{p1} curve (i.e. the $v_{\infty 1}$ level set) and the r_{p2} curve (the manifold section $\gamma_{v_{\infty 1}}^s$). In particular, the

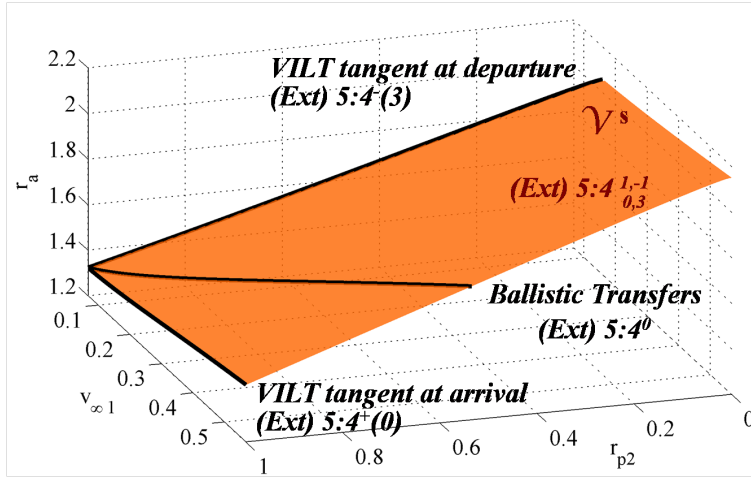


Figure 4. The manifold $\mathcal{V}^{(1,30,-1,3,+1,5)}$, set of the solutions to the $(+1) 5 : 4_{0,3}^{+1,-1}$ VILT with $v_{\infty 1} = 0.12$. The tangent VILTs $(+1) 5 : 4^{-1}(3)$ and $(+1) 5 : 4^{-1}(0)$ are at the boundary of the manifold

figure shows the tangent VILTs with two solid arrows, noting that the tangent VILTs must begin or end at $r_p = 1$. The dashed arrow is an example of non-tangent VILT.

The manifold sections can have a small fold close to $r_p = 1$, so that their numerical computation using continuation methods is often cumbersome. Therefore, we suggest using $v_{\infty 2}$ as a *continuation parameter*. For advanced continuation methods we refer to Doedel et al.¹⁷

Piecewise linear approximation

Figure 4 suggests that the manifolds \mathcal{V}^s and their sections $\gamma_{v_{\infty 1}}^s$ are almost flat (with the exception of a very small region close $r_p = 1$ not visible in the picture). Then we can approximate the curves $\gamma_{v_{\infty 1}}^s$ with linear or piecewise linear functions, which we construct using the ballistic and tangent solutions. Another approach would be to approximate the entire manifold \mathcal{V}^s with one plane; in the future we envision investigating the accuracy of this second method, which would allow the storage of a family of solution manifolds with only a few parameters.

The one-dimensional solution spaces of ballistic and tangent VILTs (non-approximated) can be computed and stored easily (much more efficiently than two-dimensional \mathcal{V}^s).¹² In what follows we assume that the families of ballistic and tangent VILTs are stored as points $r_a(v_{\infty 1}), r_{p1}(v_{\infty 1})$ for a discrete set of v_{∞} in the feasible domain $[v_{\infty 1min}, v_{\infty 1max}]$.

We can now compute a linear approximation of $\gamma_{v_{\infty 1}}^s$ for a given s and $v_{\infty 1}$. We use the stored data to retrieve (up to) three points $(r_{VA2}, r_{LA}) \in \gamma_{v_{\infty 1}}^s$:

- the ballistic solution belonging to the family of ballistic transfers $n : m^{(\sigma 1 + \sigma 2)/2}$ (the point $P2$ in the example of Figure 5).
- the VILT tangent at departure, belonging to the family of tangent VILTs $n : m^{\sigma 2, k 2}$ (the point $P3$ in the example of Figure 5).
- the VILT tangent at arrival, belonging to the family of tangent VILTs $n : m^{\sigma 1, k 1}$ (the point $P1$ in the example of Figure 5).

If $v_{\infty 1}$ is outside the allowed range $[v_{\infty 1min}, v_{\infty 1max}]$ for one family of tangent VILTs, we can still use two points to construct a linear instead of a piecewise linear approximation, as shown in Figure 6 (c). Figure

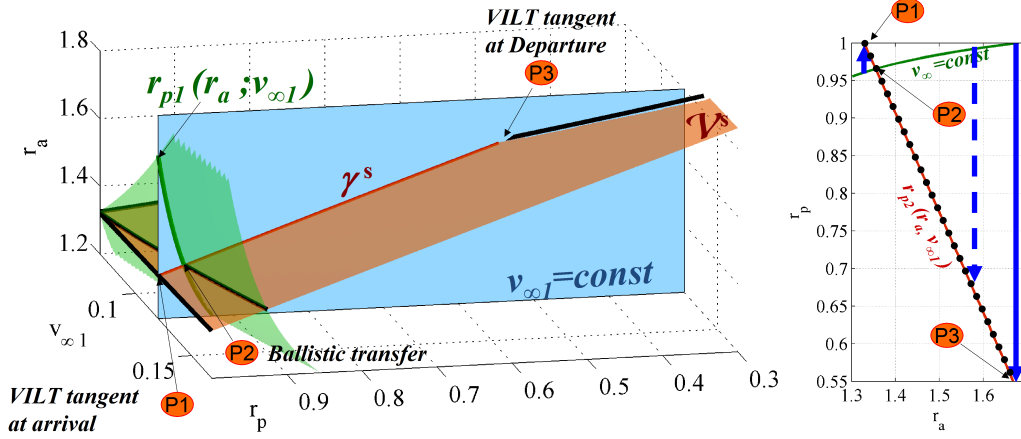


Figure 5. On the left, close up of the manifold $\mathcal{V}^{(1,0,-1,3,+1,5)}$ and its section at $v_{\infty 1} = 0.12$. On the right, the manifold section on the Tisserand graph (rotated frontal view of the section in the left). The points $P1$ and $P3$ are the tangent VILTs (represented with the vertical arrows), while $P2$ is the ballistic transfer

5 on the right shows the piecewise linear approximation with black dots. We note that the approximation completely overlaps the real solution.

For a fixed $(EI) n : m$, and for a given $v_{\infty 1}$, there are in total $4m$ curves $\gamma_{v_{\infty 1}}^s$ (one for each possible combination of σ_1, σ_2, k_1). We can compute their linear approximation by retrieving up to $3 + 2m$ stored points (one for each ballistic and tangent VILT solution). Figure 6 shows all the twelve curves $\gamma_{v_{\infty 1}}^s$ for a $(+1) 4 : 3$ VILT with $v_{\infty 1} = 0.15$. The linear approximations are the dotted curves. Note that the VILT tangent at arrival has no solution for $k_1 = 2$. In this case we only use $P1$ and $P2$ to compute the linear approximation.

DESIGN OF MULTIPLE GRAVITY ASSIST - MULTIPLE VILT TRAJECTORIES

The graphical analysis developed in the previous section forms the basis for a new design method to compute multiple gravity assist - multiple VILT trajectories.

For the sake of clarity, in this section we consider a sequence of VILTs and gravity assists at one moon only. In particular, we are interested in the design of a sequence of VILTs and gravity assists at Dione to bring the spacecraft from a point A to a point Z of the Tisserand graph in Figure 7. Our design approach however is very general and can be equally implemented to drive the spacecraft everywhere in the Tisserand graph, depending on the mission requirements. Note that a VILT provides a mechanism to efficiently change the v_{∞} . If points A and Z were on the same v_{∞} level set, the A to Z transfer could be accomplished using gravity assists only. In figure 7, the four vertical arrows represent VILTs while the arrows following the v_{∞} contours are gravity assists.

Building block

We begin the design with one building block of the trajectory, which we call a *phase*, consisting of one gravity assist and one VILT. The first phase of the Dione part of the trajectory is shown in detail in Figure 7. The point A represents the initial conditions. The gravity assist moves the spacecraft to the point B on the $v_{\infty 1}$ level set. Then the VILT moves the spacecraft to the point C on a solution curve $\gamma_{v_{\infty 1}}^s$.

How do we design this phase, i.e. how do we find the coordinates of the points B and C ? We know that B must be on the $v_{\infty 1}$ level set; in order to choose a single VILT and the associated gravity assist, we could think of plotting all the solution curves $\gamma_{v_{\infty 1}}^s$ for all the possible parameter vectors s , and choose a point on a curve satisfying some heuristic criteria (or just choose a discrete set of them). Unfortunately, for each

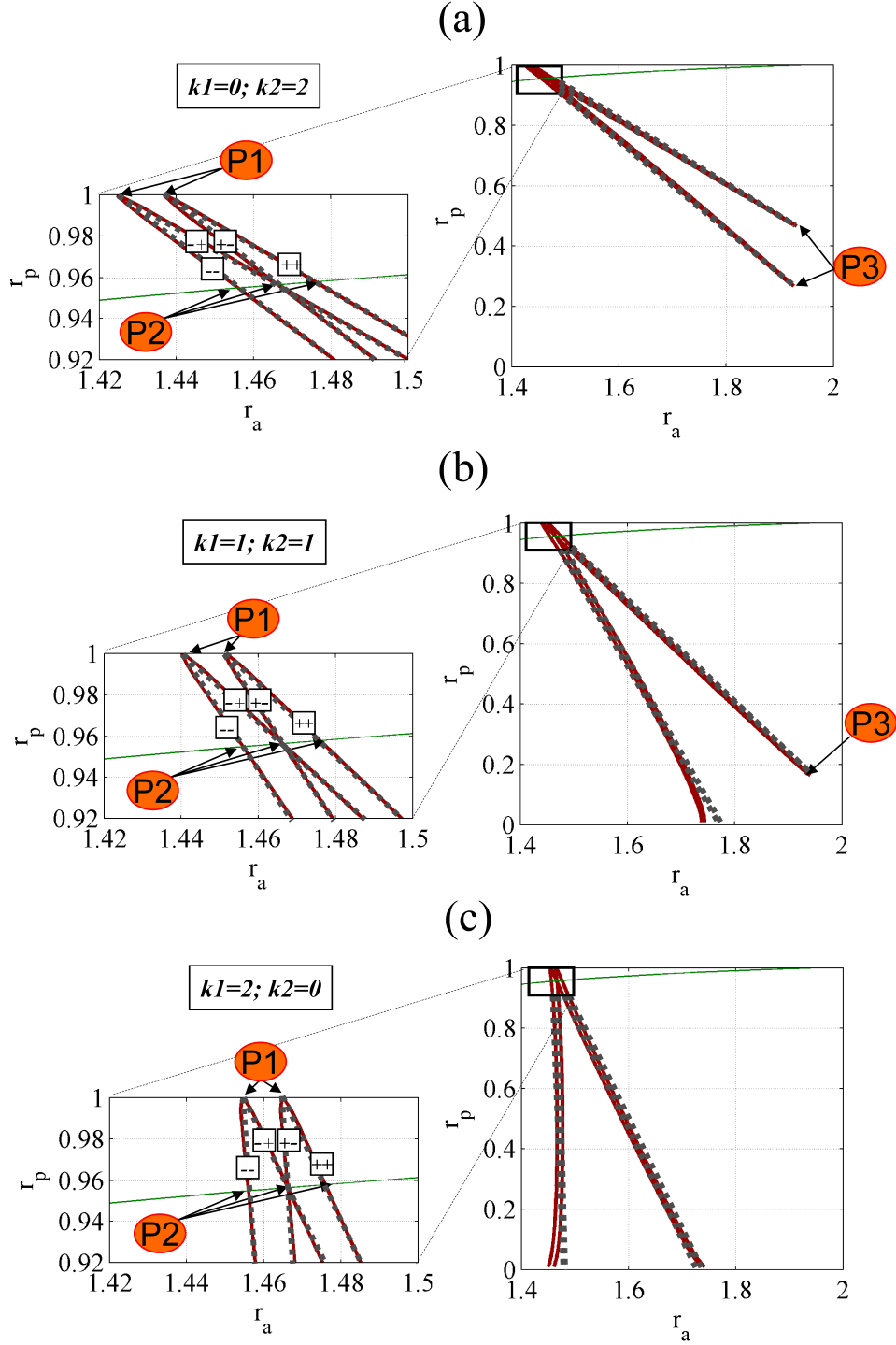


Figure 6. Numerical (solid line) and approximate (dots) solutions of the (+1) $4 : 3_{k_1, k_2}^{\sigma_1, \sigma_2}$ VILTs for $k_1 = 0$ (a), $k_1 = 1$ (b), and $k_1 = 2$ (c). The left column shows a close up of the right pictures. The signs in the box are the signs of (σ_1, σ_2) for the different curves

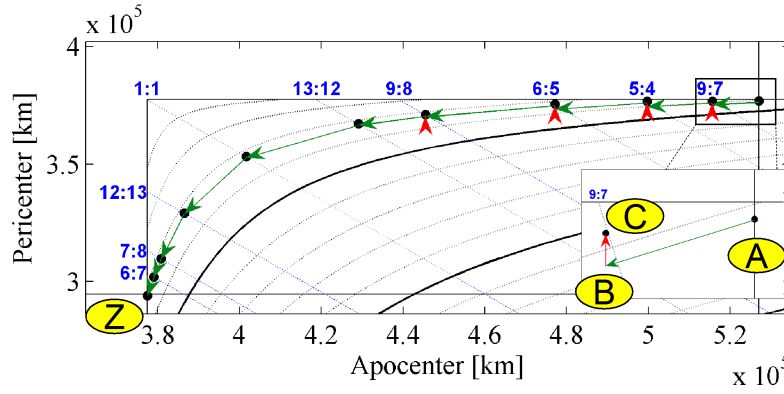


Figure 7. A sequence of gravity assists and VILTs at Dione brings the spacecraft from a Rhea-Dione transfer (point *A*) to a Dione-Tethys transfer (point *Z*). The solid line curves are v_∞ level sets (bold lines for $v_\infty = 1, 2, \dots$ km/s). The lines with slope -1 represent orbits with the same resonance. The box on the bottom right shows a close up of the first gravity assist (from *A* to *B*) and of the first VILT (from *B* to *C*)

resonant ratio $n : m$ there are $4m$ curves $\gamma_{v_\infty 1}^s$, and each point of each curve requires solving numerically Eq(11). As a result, even the calculation of a discrete set of possible C would be computationally expensive; it would also produce a clouds of points difficult to visualize and evaluate.

We tackle this problem in two steps: first we limit the time of flight of the phase, i.e. we limit the number of moon revolutions n for the VILT; second for each m we replace the associated $4m$ solutions curves with 2 piecewise linear curves computed with $m + 2$ stored data points. This second step is achieved with the following assumptions:

- We assume the gravity assists do not flip the sign of the flight path angle. Note that flipping the flight path angle results in a very large bending angle, and leads to inefficient (if not infeasible) gravity assists. To impose this condition, we put a constraint on σ_1 because $\sigma_1 EI$ is the sign of the flight path angle following the gravity assist. In particular, when patching two phases together we require $\sigma_1 EI = (-\sigma_2 EI)_{previous\ phase}$. This halves the number of $\gamma_{v_\infty 1}^s$ curves to be computed.
- We use the linearized approximation to $\gamma_{v_\infty 1}^s$ explained in the previous section; for a fixed $n : m$ and σ_1 we compute the $2m$ piecewise linear curves using $2 + m$ stored data points.
- We disregard suboptimal solutions. In particular, for each $n : m, \sigma_1, \sigma_2$ we replace the m piecewise linear curves ($k_1 = 0, \dots, m - 1$) with one piecewise linear curve, where for each r_{VA} we chose the minimum r_{LA} greater than r_{LAmin} . This last assumption is better explained in Figure 8, where we plot the $\gamma_{v_\infty 1}^s$ for $(+1) 5 : 4_{k_1, k_2}^{-1, -1}$ (with $k_1 = 0, \dots, 3; k_2 = m - k_1 - 1$) and $v_\infty = 0.3$, together with two piecewise linear curves (in bold) obtained for two different initial conditions, hence two different r_{LAmin} .

With these assumptions we compute a discrete set of possible choices for C in a very short time ($\ll 1$ second for a Matlab code on a laptop PC). We can plot the results and apply some heuristic approach to choose the next point, or loop through them in a global search algorithm like branch and bound.¹⁸

The sequence

The sequence of Dione VILTs and gravity assists in Figure 7 is designed by applying iteratively the approach explained above. The point C of the first phase becomes the new initial condition (point A) of the second phase. The last point of the last phase (the point Z) must allow a transfer to Tethys. Note that the initial and final points A and Z of the sequence are usually at different v_∞ s. In Figure 7 $\tilde{v}_\infty = 0.82$ km/s at

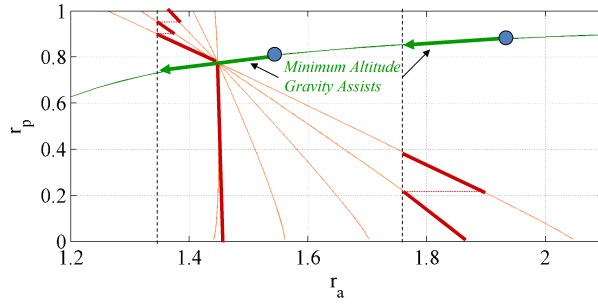


Figure 8. Five solution curves for the $(+1) 5 : 4_{k1,k2}^{-1,-1}$ VILT, and two optimal curves (piecewise linear, in bold) obtained choosing the lowest r_a for each r_p , for two different initial conditions

the initial point A , while $\tilde{v}_\infty = 0.64$ km/s at the final point Z . Accordingly, the sequence must reduce the v_∞ .

The following comments about VILTs are important for the design:

- It is more efficient to reduce or increase the v_∞ if r_{VA2} is close to 1, that is on the top (left) part of the Tisserand graph for exterior (interior) VILTs. In particular, tangent VILTs maximize the change of v_∞ for a given Δv^{12} (under the assumption of tangent burns at the apse).
- In direct contrast to the previous bullet, the gravity assist is least efficient in reducing or increasing semi-major axis if r_{VA1} is close to 1 (see Figure 1). As a consequence, tangent and near-tangent VILTs have an adverse affect on total transfer time. Therefore the design is a careful trade study balancing the fuel efficiency of tangent VILTs with the time efficiency of non-tangent gravity assists.
- A Δv which increases (decreases respectively) v_∞ can lead to a desired decrease (increase) of semi-major axis. In some cases the only way to reach a short time-of-flight resonance is to accept an increase (decrease) in v_∞ .
- Minimum altitude gravity assists always lead to the largest change in r_a and r_p .
- Minimum altitude gravity assists do not always reduce the total transfer time. In some cases a higher altitude gravity assist can lead to a VILT with a preferred resonance (i.e. with a lower n).

Using these comments and the graphical method presented, we design the transfer in Figure 7 in a few steps.

Example of design

Using the assumptions and comments presented in the last sections, we design the first phase of the Dione part of the trajectory. The initial conditions and general assumptions are the following:

- The initial apocenter relative to Saturn is 527,063 km and the initial pericenter is 377,000 km, and $\tilde{v}_{\infty 1} = 0.82$ km/s.
- The flight path angle before the gravity assist is positive, which means that the first arc of the VILT must be short ($\sigma_1 = -1$).
- The maximum VILT time of flight is chosen as approximately 36 days, that is: $n < 14$ (the period of Dione is 2.74 days)
- The minimum gravity-assist altitude for the first encounter is 100 km and 50 km for the following gravity assists. A minimum-altitude gravity assists leads to the minimum r_a of 510,495 km.

Figure 9 shows the initial condition (point A) and the $\tilde{v}_{\infty 1}$ level set. It also shows some piecewise linear curves marked with empty triangles or filled circles. In the area of interest there are only three $n : m$ VILTs with $n < 14$. The 13 : 10 VILTs are the two curves on the right, the 9 : 7 VILTs are the two curves in the center, and the 5 : 4 VILTs are the two curves on the left.

A possible choice for the design of this phase consists of a gravity assist from A to B' , followed by a VILT from B' to C' . This choice has the advantage to decrease the apocenter the most, with a short time of flight of approximately 5 Dione revolutions. However, in order to reach the 5 : 4 VILT it is necessary to apply quite a large Δv (indicated by the large vertical displacement) and increase the v_{∞} .

A different option is to make a gravity assist to from A to B , and a VILT from B to C which lies on the $\sigma_2 = -1$ curve. The transfer time is almost twice that of the previous option, however the Δv is much smaller and also results in a desired decrease of v_{∞} . In this case we choose the second option, because it represents a better compromise in the Δv vs. time-of-flight trade; however it is clear that both presented options, and probably a few more, might be considered for an exhaustive search of trajectory options. Note that the point C is close to but not exactly at $r_p = 1$, where the Δv decreases the v_{∞} the most¹² but the zero flight-path angle is the least efficient for an energy changing gravity assist.

Once we select C as the chosen solution, we are ready to design the second phase, with $A_{new} = C$ and $\sigma_{1new} = -\sigma_2 = +1$. We apply this design approach iteratively to find the sequence of gravity assists and VILTs shown in Figure 7.

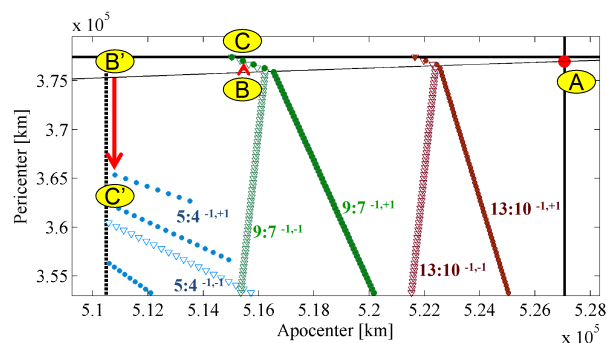


Figure 9. Discrete sets of possible choices for the design of the first phase of the sequence of VILTs at Dione. The curves with filled circles represents VILTs with $(\sigma_1, \sigma_2) = (-1, +1)$. The curves with empty triangles represents VILTs with $(\sigma_1, \sigma_2) = (-1, -1)$. The chosen design ABC consists of a 350 km altitude gravity assist and of a 4.7 m/s VILT

ENCELADUS ORBITER TRAJECTORY DESIGN

Using the methodology presented in the previous section, we design a trajectory from a highly elliptical orbit around Saturn (from the orbit following the pericenter raise maneuver in the Titan Saturn System Mission¹⁹) to a 200 km altitude orbit around Enceladus. The trajectory comprises 52 gravity assists and VILTs at Titan, Rhea, Dione, Tethys and Enceladus, for a total time of flight $tof \sim 2.7$ years and a total Δv of ~ 450 m/s including the Enceladus Orbit Insertion (EOI). We stress that this Δv is almost ten times less than the Titan- Enceladus Hohmann transfer Δv .

We split the trajectory into five legs : Titan , Rhea , Dione , Tethys , and Enceladus. Each leg is composed of gravity assists and VILTs at one moon only. The final conditions of each leg are taken as initial conditions for the following leg; Note that we do not design the transfer connecting two consecutive legs, which is considered beyond the scope of the paper and is expected to give small contributions to the total time of flight (a few revolutions of the gravity-assist moon) and total Δv .

The time of flights and total Δv s are recomputed solving the numerical VILTs, showing an agreement with the approximate piecewise linear VILT values within 3.3% (less than 0.02 % in most cases).

Figures 7 and 10-13 show the Tisserand graphs of the different legs of the trajectory, while Figures 14-18 show the trajectory in the $x - y$ plane. In each plot, the star is the location of the first flyby, while the circle is the location of the last flyby. Tables 2-6 show the Δv , gravity assist altitude, and the time of flight of all the phases of each leg. Table 7 summarizes the total Δv and time of flight for each phase. We compare the solution described above to a second solution we found previously with a larger Δv and shorter time of flight. This second solution was presented in Strange et al.¹⁰ We also compare both solutions with a Titan-Enceladus Hohmann transfer. For completeness we also show the Δv for the Saturn Orbit Insertion (SOI) and Pericenter Raise Maneuver (PRM) and the associated time of flight.

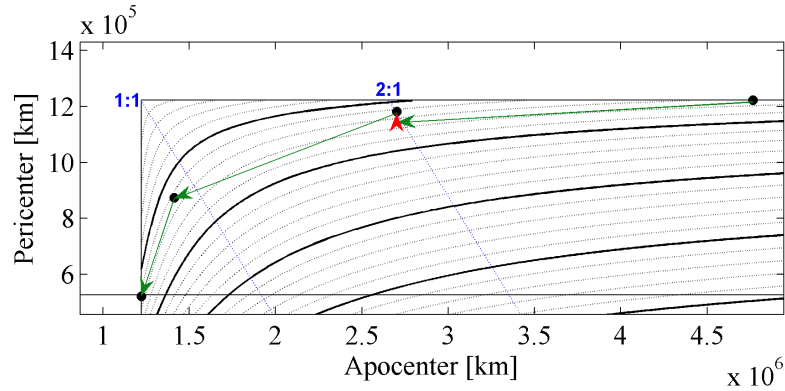


Figure 10. VILTs and gravity assists at Titan. The solid line curves are v_∞ level sets (bold lines for $v_\infty = 1, 2, \dots$ km/s). The lines with slope -1 represent orbits with the same resonance

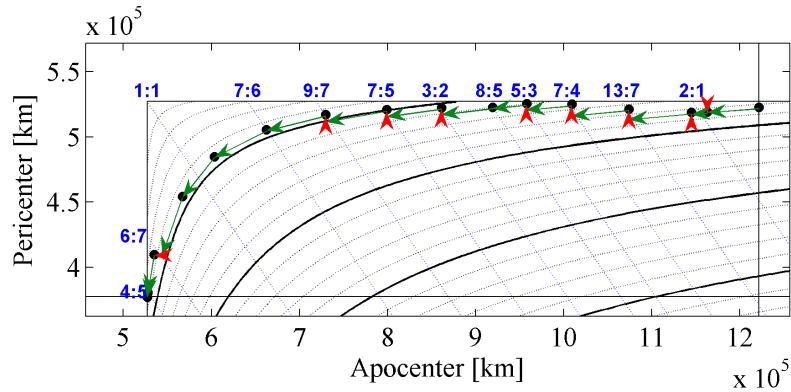


Figure 11. VILTs and gravity assists at Rhea. The solid line curves are v_∞ level sets (bold lines for $v_\infty = 1, 2, \dots$ km/s). The lines with slope -1 represent orbits with the same resonance

CONCLUSION

In this paper we study the solution space of the general V-Infinity Leveraging Transfer (VILT) problem and demonstrate that the space is almost flat for a proper choice of coordinates. We derive an approximation to the solution space which allows for fast computation of the transfers and associated design space searches. This linear approximation is the first important result of the paper. Using the approximation and the Tisserand graphs, we introduce a fast graphical design method for multiple-VILT transfers. This new design method is the second important result of this paper. Using the new method we quickly and easily compute a trajectory from a highly eccentric orbit at Saturn to a 200 km orbit at Enceladus. The trajectory includes 52 gravity assists at Titan, Rhea, Dione, Tethys and Enceladus. The time of flight is 2.7 years, and the total Δv is

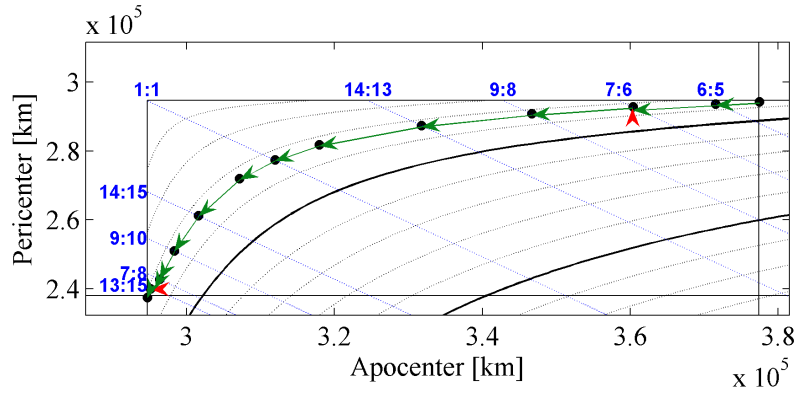


Figure 12. VILTs and gravity assists at Tethys.The solid line curves are v_{∞} level sets (bold lines for $v_{\infty} = 1, 2, \dots$ km/s). The lines with slope -1 represent orbits with the same resonance

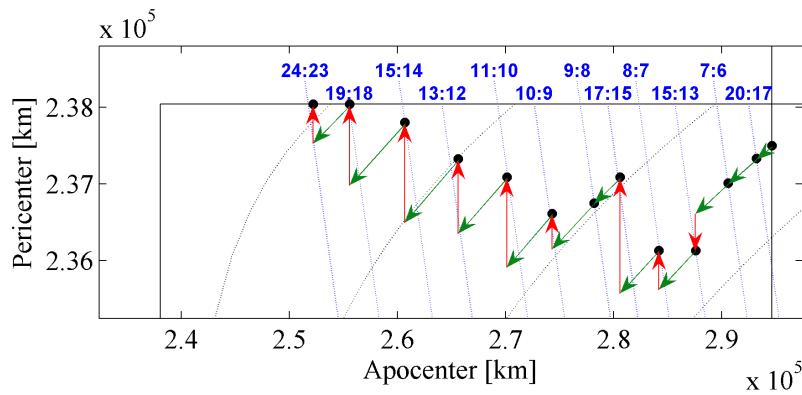


Figure 13. VILTs and gravity assists at Enceladus.The solid line curves are v_{∞} level sets. The lines with slope -1 represent orbits with the same resonance

Table 2. Titan leg

Flyby	tof [d]	Altitude [km]	Transfer Type	$v_{\infty 1}$ [km/s]	$v_{\infty 2}$ [km/s]	ΔV [m/s]
Titan-1	31.4	2280	(+1) 2 : 1 _{0,0} ^{-1,+1}	1.46	1.26	28.8
Titan-2	21.3	3000	1 : 1 ^{+1,+1}	1.26	1.26	0.0
Titan-3	—	15090	<i>transfer to Rhea</i>			

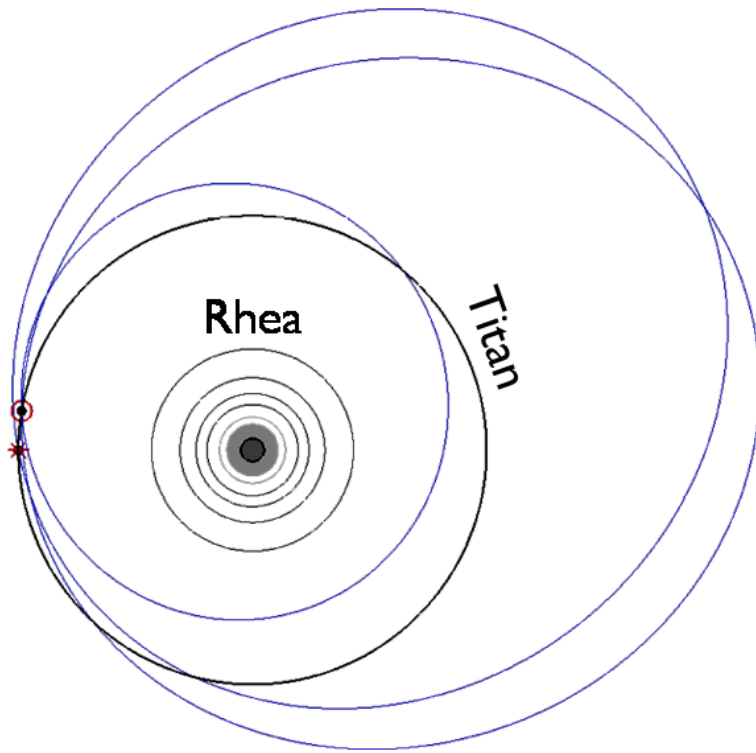


Figure 14. VILTs and gravity assists at Titan

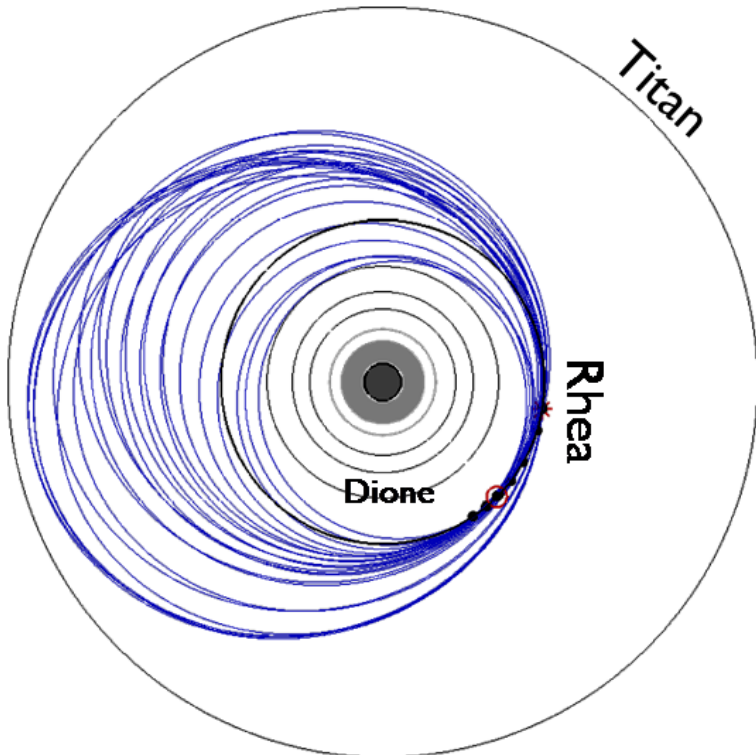


Figure 15. VILTs and gravity assists at Rhea

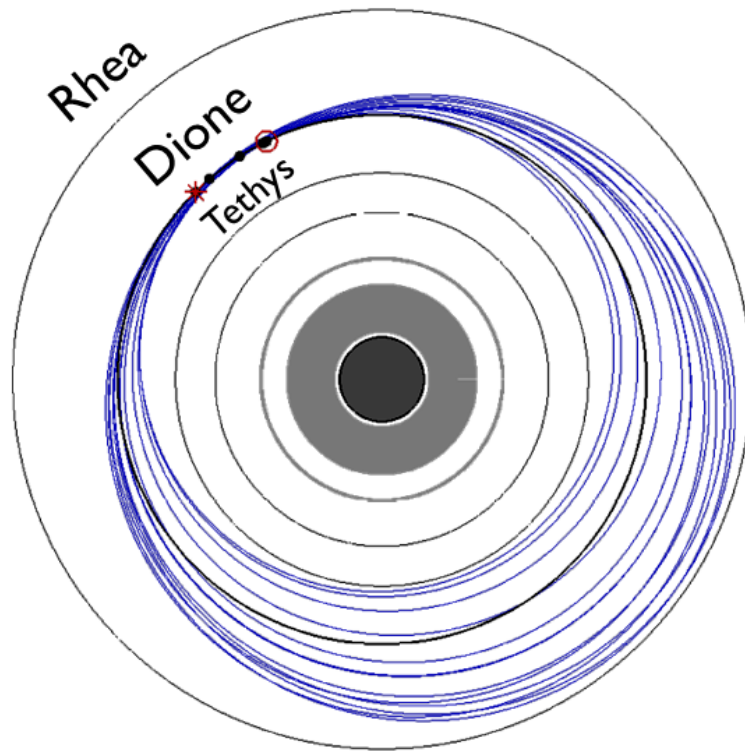


Figure 16. VILTs and gravity assists at Dione

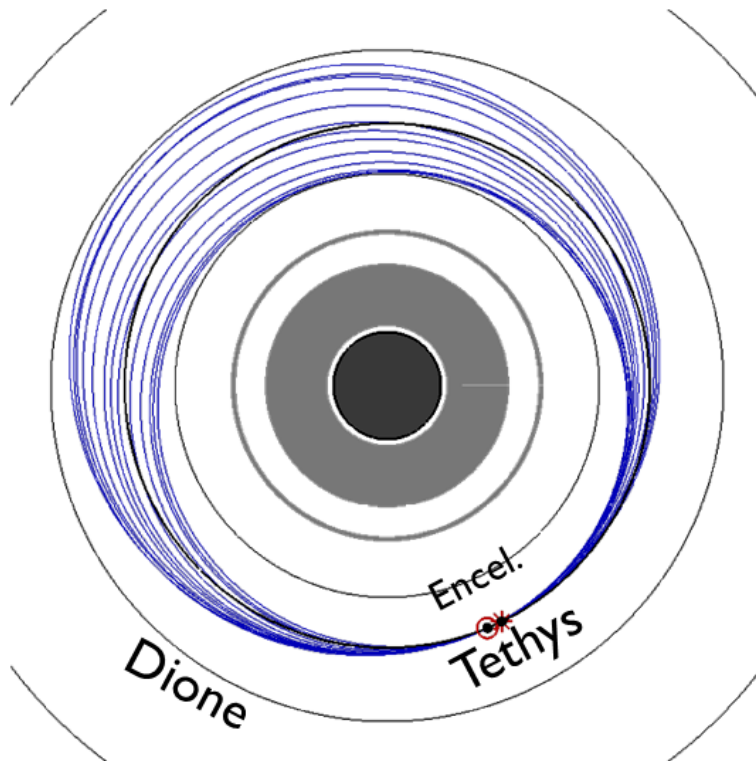


Figure 17. VILTs and gravity assists at Tethys

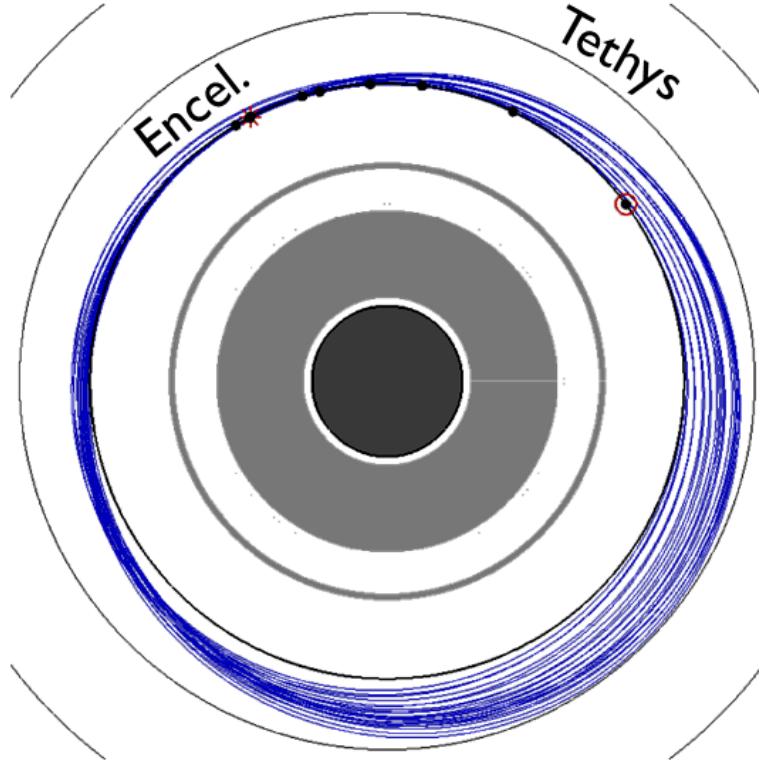


Figure 18. VILTs and gravity assists at Enceladus

Table 3. Rhea leg

Flyby	tof [d]	Altitude [km]	Transfer Type	$v_{\infty 1}$ [km/s]	$v_{\infty 2}$ [km/s]	ΔV [m/s]	
Rhea-1	9.5	100	(+1) 2 : $1_{0,0}^{+1,+1}$	1.66	1.68	1.9	
Rhea-2	17.5	2510	(+1) 2 : $1_{0,0}^{-1,-1}$	1.68	1.67	1.4	
Rhea-3	59.2	60	(+1) 13 : $7_{1,5}^{+1,+1}$	1.67	1.50	21.5	
Rhea-4	39.1	70	(+1) 7 : $4_{2,1}^{-1,-1}$	1.50	1.30	25.1	
Rhea-5	22.7	70	(+1) 5 : $3_{0,2}^{+1,-1}$	1.30	1.20	12.7	
Rhea-6	36.1	270	8 : $5^{+1,-1}$	1.20	1.20	0.0	
Rhea-7	13.6	150	(+1) 3 : $2_{0,1}^{+1,-1}$	1.20	1.09	14.6	
Rhea-8	31.7	150	(+1) 7 : $5_{0,4}^{+1,-1}$	1.09	0.99	15.2	
Rhea-9	40.7	120	(+1) 9 : $7_{0,6}^{+1,-1}$	0.99	0.90	16.9	
Rhea-10	31.6	230	7 : $6^{+1,-1}$	0.90	0.90	0.0	
Rhea-11	6.5	220	1 : $1^{+1,+1}$	0.90	0.90	0.0	
Rhea-12	6.2	310	1 : $1^{+1,+1}$	0.90	0.90	0.0	
Rhea-13	30.2	60	(-1) 6 : $7_{6,0}^{-1,-1}$	0.90	0.74	37.2	
Rhea-14	18.1	50	4 : $5^{+1,-1}$	0.74	0.74	0.0	
Rhea-15	—	3660	<i>transfer to Dione</i>				

Table 4. Dione leg

Flyby	tof [d]	Altitude [km]	Transfer Type	$v_{\infty 1}$ [km/s]	$v_{\infty 2}$ [km/s]	ΔV [m/s]
Dione-1	28.0	350	(+1) 9 : $7_{0,6}^{-1,-1}$	0.82	0.78	4.7
Dione-2	13.7	270	(+1) 5 : $4_{0,3}^{+1,-1}$	0.78	0.71	10.3
Dione-3	16.5	100	(+1) 6 : $5_{0,4}^{+1,-1}$	0.71	0.65	9.3
Dione-4	24.6	60	(+1) 9 : $8_{0,7}^{+1,-1}$	0.65	0.64	1.9
Dione-5	35.6	960	13 : $12^{+1,-1}$	0.64	0.64	0.0
Dione-6	2.7	120	1 : $1^{+1,-1}$	0.64	0.64	0.0
Dione-7	32.8	60	12 : $13^{-1,+1}$	0.64	0.64	0.0
Dione-8	19.2	190	7 : $8^{-1,+1}$	0.64	0.64	0.0
Dione-9	16.4	970	6 : $7^{-1,+1}$	0.64	0.64	0.0
Dione-10	—	620	<i>transfer to Tethys</i>			

Table 5. Tethys leg

Flyby	tof [d]	Altitude [km]	Transfer Type	$v_{\infty 1}$ [km/s]	$v_{\infty 2}$ [km/s]	ΔV [m/s]
Tethys-1	13.4	250	6 : $5^{-1,-1}$	0.70	0.70	0.0
Tethys-2	13.2	60	(+1) 7 : $6_{0,5}^{+1,-1}$	0.70	0.66	6.0
Tethys-3	17.0	60	9 : $8^{+1,-1}$	0.66	0.66	0.0
Tethys-4	26.4	70	14 : $13^{+1,-1}$	0.66	0.66	0.0
Tethys-5	2.7	60	1 : $1^{+1,+1}$	0.66	0.66	0.0
Tethys-6	1.9	640	1 : $1^{+1,-1}$	0.66	0.66	0.0
Tethys-7	2.6	610	1 : $1^{+1,+1}$	0.66	0.66	0.0
Tethys-8	26.4	80	14 : $15^{-1,+1}$	0.66	0.66	0.0
Tethys-9	17.0	90	9 : $10^{-1,+1}$	0.66	0.66	0.0
Tethys-10	13.2	100	7 : $8^{-1,+1}$	0.66	0.66	0.0
Tethys-11	24.5	1020	(-1) 13 : $15_{14,0}^{-1,+1}$	0.66	0.63	6.2
Tethys-12	—	860	<i>transfer to Enceladus</i>			

Table 6. Enceladus leg

Flyby	tof [d]	Altitude [km]	Transfer Type	$v_{\infty 1}$ [km/s]	$v_{\infty 2}$ [km/s]	ΔV [m/s]
Enceladus-1	27.4	240	20 : $17^{+1,-1}$	0.70	0.70	0.0
Enceladus-2	9.6	50	7 : $6^{+1,-1}$	0.70	0.70	0.0
Enceladus-3	20.7	50	(+1) 15 : $13_{4,8}^{+1,+1}$	0.70	0.74	6.1
Enceladus-4	12.3	50	(+1) 8 : $7_{3,3}^{-1,-1}$	0.74	0.70	6.5
Enceladus-5	23.3	50	(+1) 17 : $15_{1,13}^{+1,-1}$	0.70	0.59	19.3
Enceladus-6	12.3	190	9 : $8^{+1,-1}$	0.59	0.59	0.0
Enceladus-7	13.9	50	(+1) 10 : $9_{0,8}^{+1,+1}$	0.59	0.56	5.8
Enceladus-8	16.4	50	(+1) 11 : $10_{0,9}^{-1,-1}$	0.56	0.47	15.1
Enceladus-9	18.0	50	(+1) 13 : $12_{8,3}^{+1,+1}$	0.47	0.40	12.5
Enceladus-10	20.5	50	(+1) 15 : $14_{0,13}^{-1,+1}$	0.40	0.30	16.8
Enceladus-11	25.9	50	(+1) 19 : $18_{1,16}^{-1,+1}$	0.30	0.22	13.6
Enceladus-12	32.8	50	(+1) 24 : $23_{19,3}^{-1,+1}$	0.22	0.18	6.4

Table 7. Trajectory comparison

	New tour		Tour from Strange et al. ¹⁰		Titan-Enceladus	
	Δv [m/s]	<i>tof</i> [days]	Δv [m/s]	<i>tof</i> [days]	Δv [m/s]	<i>tof</i> [days]
SOI+PRM	1,310	—	1,310	—	1,292	—
Titan tour	29	53	27	53	0	~ 50
Rhea tour	146	363	251	304	—	—
Dione tour	26	190	90	108	—	—
Tethys tour	12	158	28	134	—	—
Encel. tour	102	233	96	144	—	—
EOI	129	—	242	—	3,933	—
Tours + EOI	445	997 (2.7 y)	734	743 (~ 2.0 y)	3,933	~ 50

only 445 m/s, including the Enceladus orbit insertion. For comparison, the Enceladus orbit insertion from a Titan-Enceladus Hohmann transfer is almost 4 km/s. The low Δv and flight time solutions presented in this study embolden the already strong arguments to send an orbiter to Enceladus. The new method and demonstrated results generally apply to any mission that tours and ultimately orbits small mass moons. This class of high-science-value missions was previously considered impractical due to flight time and delta v constraints.

ACKNOWLEDGMENTS

Part of the research in this paper was carried out at the Jet Propulsion Laboratory, California Institute of Technology, under contract with the National Aeronautics and Space Administration.

NOTATION

α Pump angle between the v_∞ vector and the minor body velocity vector

δ Turning angle between the incoming and outgoing v_∞ vectors of a gravity assist

$\gamma_{v_\infty 1}^s$ Section of the VILT solution manifold for a given s and $v_\infty 1$

$\Delta\theta$ Spacecraft angular gain

σ_i Element of s : if +1 denotes a long i th arc, if -1 denotes a short i th arc

μ_M, μ_P Gravitational parameter of the minor and major body

EI Element of s : if +1 denotes exterior VILTs, if -1 denotes interior VILTs

f, E, M True, eccentric and mean anomaly of the spacecraft with respect to the major body

n Number of minor body revolutions during the VILT

m Number of major body revolutions during the VILT

k_i Element of s : number of full revolutions in the i th arc

r_π Pericenter of the gravity assist hyperbola

r_a, r_p, a Apocenter, pericenter and semi-major axis of the spacecraft with respect to the major body

r_{LA}, r_{VA} Leveraging and vacant apses of the spacecraft with respect to the major body, i.e. the furthers and closest apse to $r = 1$ respectively

s VILT parameter vector; in particular $s = (\sigma_1, k_1, \sigma_2, k_2, n, EI)$

v_p, v_a Velocity of the spacecraft at pericenter and at apocenter with respect to the major body

v_∞ Velocity of the spacecraft relative to the moon at $r = 1$

\mathcal{V}^s VILT solution manifold

1, 2 Subscripts indicates the first or second arc

REFERENCES

- [1] S. N. Williams, "Automated Design of Multiple Encounter Gravity-Assist Trajectories," Master's thesis, Purdue University, School of Aeronautics and Astronautics, West Lafayette, IN, Aug. 1990.
- [2] C. Uphoff, P. H. Roberts, and L. D. Friedman, "Orbit Design Concepts for Jupiter Orbiter Missions," *AIAA Mechanics and Control Conference, Anaheim, California*, Aug. 1974. AIAA Paper 74-781.
- [3] R. W. Farquhar, D. W. Dunham, and J. V. McAdams, "NEAR mission overview and trajectory design," *Journal of the Astronautical Sciences*, Vol. 43, No. 4, 1995, pp. 353–371.
- [4] T. D. Goodson, D. L. Gray, and Y. Hahn, "Cassini Maneuver Experience: Launch And Early Cruise," *AIAA Guidance, Navigation, & Control Conference, Boston, MA*, Aug. 1998. AIAA Paper 98-4224.
- [5] T. D. Kowalkowski, J. R. Johannesen, and L. Try, "Launch Period Development for the Juno Mission to Jupiter," *AIAA/AAS Astrodynamics Specialist Conference and Exhibit, Honolulu, Hawaii*, 2008. Paper AIAA-2008-7369.
- [6] J. V. McAdams, D. W. Dunham, R. W. Farquhar, A. H. Taylor, and B. G. Williams, "Trajectory design and maneuver strategy for the MESSENGER mission to mercury," *Journal of Spacecraft and Rockets*, Vol. 43 5, 2006, pp. 1054–1064. doi: 10.2514/1.18178.
- [7] G. Hollenbeck, "New Flight Techniques for Outer Planet Missions," *AAS Microfishes series*, Vol. 26, 1975. Supplement to the *Advances in the Astronautical Sciences*, Vol. 33, Univelt, San diego, also AAS Paper 75-087.
- [8] J. A. Sims, J. M. Longuski, and A. Staugler, "V-infinity Leveraging for Interplanetary Missions: Multiple-Revolution Orbit Techniques," *Journal of Guidance, Control, and Dynamics*, Vol. 20, No. 3, 1997, pp. 409–415. doi: 10.2514/2.4064.
- [9] N. J. Strange and J. A. Sims, "Methods for the design of V-infinity leveraging maneuvers," *Advances in the Astronautical Sciences*, Vol. 109, Univelt, San Diego, 2001, pp. 1959–1976. also Paper AAS 01-437.
- [10] N. J. Strange, S. Campagnola, and R. P. Russell, "Leveraging Flybys of Low Mass Moons to Enable an Enceladus Orbiter," *Proceedings of the Astrodynamics Specialist Conference, Pittsburgh, PA*, Aug 2009. Paper AAS 09-435. Submitted to *Journal of Spacecraft and Rockets*.
- [11] A. T. Brinkerhoff and R. P. Russell, "Pathfinding and V-Infinity Leveraging for Planetary Moon Tour Missions," *Proceeding of the AAS/AIAA Space Flight Mechanics Meeting, Savannah, GA*, Feb 2009. Paper AAS 09-222.
- [12] S. Campagnola and R. P. Russell, "Endgame Problem Part 1: V-Infinity Leveraging Technique and Leveraging Graph," *Journal of Guidance, Control, and Dynamics.*, Vol. 33, Mar/Apr 2010, p. 463475.
- [13] S. Campagnola and R. P. Russell, "Endgame Problem Part 2: Multi-Body Technique and T-P Graph," *Journal of Guidance, Control, and Dynamics.*, Vol. 33, Mar/Apr 2010, p. 476486.
- [14] M. Vasile and S. Campagnola, "Design of Low-Thrust Multi-Gravity Assist Trajectories to Europa," *Journal of the British Interplanetary Society*, Vol. 62, Jan 2009, pp. 15–31.
- [15] R. Abraham, J. E. Marsden, and T. S. Ratiu, *Manifold, Tensor, Analysis, and Applications*, pp. 107–108 and 174–175. Springer, 1988.
- [16] A. Labunsky, O. Papkov, and K. Sukhanov, *Multiple Gravity Assist Interplanetary Trajectories*, pp. 33–68. Earth Space Institute Book Series, Gordon and Breach Publishers, London, 1998.
- [17] E. J. Doedel, H. B. Keller, and J. P. Kernévez, "Numerical Analysis and Control of Bifurcation Problems: (I) Bifurcation in Finite Dimension," *International Journal of Bifurcation and Chaos*, Vol. 1, No. 3, 1991, pp. 493–520.
- [18] A. H. Land and A. G. Doig, "An Automatic Method of Solving Discrete Programming Problems," *Econometrica*, Vol. 28, Jul 1960, pp. 497–520.
- [19] N. J. Strange, T. L. Spilker, D. F. Landau, T. Lam, D. T. Lyons, and J. J. Guzman, "Mission Design for the Titan Saturn System Mission Concept," *Astrodynamics Specialist Conference, Pittsburgh, PA*, Aug. 2009. Paper AAS 09-356.